

Influence of monolayer contamination on electric-field-noise heating in ion trapsA. Safavi-Naini,^{1,2} E. Kim,³ P. F. Weck,⁴ P. Rabl,⁵ and H. R. Sadeghpour²¹*Department of Physics, Massachusetts Institute of Technology, Cambridge, Massachusetts 02139, USA*²*ITAMP, Harvard-Smithsonian Center for Astrophysics, Cambridge, Massachusetts 02138, USA*³*Department of Physics and Astronomy, University of Nevada, Las Vegas, Nevada 89154-4002, USA*⁴*Sandia National Laboratories, P.O. Box 5800, Albuquerque, New Mexico 87185-0779, USA*⁵*Institute of Atomic and Subatomic Physics, TU Wien, Stadionallee 2, 1020 Wien, Austria*

(Received 1 October 2012; published 22 February 2013)

Electric field noise is a hinderance to the assembly of large-scale quantum computers based on entangled trapped ions. Apart from ubiquitous technical noise, experimental studies of trapped ion heating have revealed additional limiting contributions to this noise, originating from atomic processes on the electrode surfaces. In a recent work [Safavi-Naini, Rabl, Weck, and Sadeghpour, *Phys. Rev. A* **84**, 023412 (2011)] we described a microscopic model for this excess electric field noise, which points a way towards a more systematic understanding of surface adsorbates as progenitors of electric field jitter noise. Here, we address the impact of surface monolayer contamination on adsorbate-induced noise processes. Using exact numerical calculations for H and N atomic monolayers on a Au(111) surface, representing opposite extremes of physisorption and chemisorption, we show that an additional monolayer can significantly affect the noise power spectrum and, respectively, enhance and suppress the heating rates.

DOI: [10.1103/PhysRevA.87.023421](https://doi.org/10.1103/PhysRevA.87.023421)

PACS number(s): 37.10.Ty, 34.35.+a, 37.10.Rs, 72.70.+m

I. INTRODUCTION

Ion trap miniaturization and a precise control of errors in the entangled qubits are two key prerequisites for using trapped laser-cooled atomic ions as multiqubit logic gates in a scalable quantum architecture [1–3]. One main source of qubit error in such systems is the motional jitter of the collective behavior of the ions in microtraps [4–13]. Some of the unwanted heating noise is naturally mitigated by operating the traps at cryogenic temperatures [7,9,10]. However the noise still remains larger than the expected Johnson noise for the traps. Early observations of the dependence of the heating rate on the position of the ions above the trap ($\sim 1/d^4$) [5–7] and on the elapsed time in the ion-loading region [4,5] lend credence to the role played by surface contaminants. Further experiments with superconducting traps [10] corroborate the understanding that the noise source lies on the surface and not in the bulk. The confirmation has come more directly from two recent and complimentary experiments, where laser cleaning [12] and ion beam bombardment [13] of the trap electrodes led to a reduction of the noise. The experiment reported in Ref. [13] also identified the surface contaminants as carbon based, in the form of two to three monolayers (MLs) of hydrocarbons.

Theoretical studies of the anomalous heating have been largely phenomenological, aiming to explain the signatures of this noise. These models use the concept of patch potentials developed by Turchette *et al.* [5] to explain the motional heating in ions [11,14,15]. In a recent work [16] we developed a microscopic model to predict the features of electric field noise (distance, frequency, and temperature dependencies) from the details of atomic surface processes. This model is predicated on the idea that the noise in ion traps emanates from a random distribution of fluctuating dipoles associated with individual adatoms on a metallic electrode surface.

In this work we extend our earlier theoretical treatment by investigating the dependence of this surface noise on the

presence of an additional ML of atomic species on a gold surface. To do so we present detailed numerical calculations on the adsorbate surface potential in the presence or absence of MLs with different reactivities. To this end, we choose He as the ML atom to represent weak binding (physisorbed species) and N as the ML atom to represent strong binding (chemisorbed species). For computational simplicity we choose hydrogen (H) as our adsorbate and compare the binding potential of H-Au(111), H-He-Au(111), and H-N-Au(111). Using density functional theory (DFT) we obtain accurate data for these surface potentials, induced dipole moments, and modifications of the phonon density of states. Combined with the semianalytical treatment of Ref. [16] we use this data to extrapolate the resulting impact on phonon-induced dipole fluctuations and find that MLs of different reactivities can lead to the completely opposite effects of reducing or enhancing the noise.

The remainder of the paper is structured as follows. In Sec. II we briefly review the problem of anomalous heating in ion traps and summarize the basic assumptions of the model detailed in Ref. [16]. As the main part of this work we present in Sec. III our numerical results on adatom surface potentials and induced dipole moments for two different types of MLs on Au. Finally, in Sec. IV we discuss the impact of these findings on the adatom dipole fluctuation spectrum, and we present our conclusions in Sec. V.

II. ANOMALOUS ION HEATING FROM FLUCTUATING SURFACE DIPOLES

In microfabricated surface ion traps, which are currently developed for quantum-information processing, single or multiple ions are trapped by electric potentials at a distance d of a few 100 μm above a metal electrode. The resulting trapping frequencies are typically around $\omega_i \sim 1$ MHz and allow efficient laser cooling and coherent manipulations of

the trapped ion. However, when cooled close to the quantum ground state of the trap, the ion motion is still associated with a large electric transition dipole moment $d_I \approx qa_0$, where q is the charge and $a_0 = \sqrt{\hbar/(2m_I\omega_I)}$ the zero-point motion for an ion mass m_I . Fluctuating electric fields from the environment couple to this dipole moment and excite the ion motion with a characteristic heating rate [5],

$$\Gamma_h = \frac{q^2}{2m_I\hbar\omega_I} S_E(\omega = \omega_I), \quad (1)$$

where $S_E(\omega)$ is the fluctuation spectrum of the electric field at the position of the ion. Since Γ_h limits the time for performing coherent manipulation of the ion, a detailed understanding of $S_E(\omega)$, its distance, frequency, and temperature dependence, is of central importance for a further optimization and miniaturization of ion microtraps.

As the trapping distance d is decreased the ion becomes increasingly more sensitive to electric noise emerging from microscopic processes on the surface. In Ref. [16] we developed a microscopic model to describe the electric field noise, which is generated from a random distribution of adatoms on a gold surface. In this case the field fluctuation spectrum for a planar trap geometry is given by

$$S_E(\omega_I) = \frac{3\pi}{4} \frac{\sigma}{(4\pi\epsilon_0)^2} \frac{S_\mu(\omega_I)}{d^4}, \quad (2)$$

where σ is the surface density of dipoles and $S_\mu(\omega) = \int_{-\infty}^{\infty} d\tau [\langle \mu_z(\tau)\mu_z(0) \rangle - \langle \mu_z(0) \rangle^2] e^{i\omega\tau}$ is the spectrum of an individual fluctuating dipole. Equation (2) predicts the expected d^{-4} scaling and together with Eq. (1) it relates the ion heating rate to the microscopic dynamics of individual surface impurities.

A. Phonon-induced dipole fluctuations of adatoms

Figure 1(a) shows a typical adatom-surface potential, $U(z)$, which is attractive at large distances z and has a sharp repulsive wall when the electronic wave functions of the adatom and the surface atoms start to overlap. The adatom-surface interaction is associated with a distortion of the electronic wave functions which results in an induced dipole moment $\mu_z(z)$ perpendicular to the surface. At large distances one expects $\mu(z) \sim 1/z^4$ [17] and $\mu(z \approx z_0)$ can reach several Debye when the adatom touches the surface.

The potential $U(z)$ usually supports several bound vibrational states $|n\rangle$ with vibrational frequencies ν_n and the adatom can undergo phonon-induced transitions between those vibrational states. For $n > m$ the corresponding transition rates are approximately given by [16]

$$\Gamma_{n \rightarrow m} = \frac{\pi g(\nu_{nm})}{3\hbar M \nu_{nm}} |\langle n|U'(z)|m\rangle|^2 [n(\nu_{nm}) + 1], \quad (3)$$

$$\Gamma_{m \rightarrow n} = \frac{\pi g(\nu_{nm})}{3\hbar M \nu_{nm}} |\langle n|U'(z)|m\rangle|^2 n(\nu_{nm}). \quad (4)$$

Here M is the surface atom mass; $g(\omega)$ is the phonon density of states (PDOS) and $n(\omega) = 1/(e^{\hbar\omega/(k_B T)} - 1)$ is the thermal phonon occupation number, which are both evaluated at the vibrational transition frequency $\nu_{nm} = \nu_n - \nu_m > 0$. Due to the different average dipole moments $\mu_n = \langle n|\mu_z|n\rangle$ associated with each vibrational state, absorption and emission

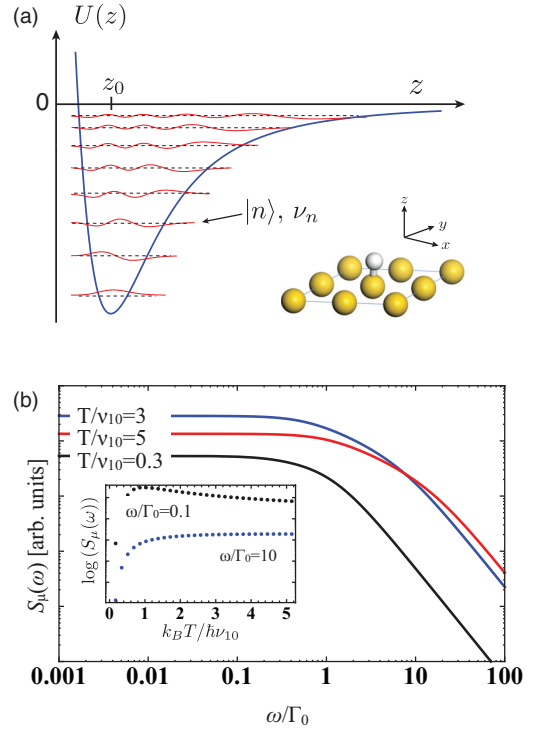


FIG. 1. (Color online) (a) A schematic binding potential $U(z)$ of an adsorbate on a bare Au surface as a function of the adatom-surface distance z . The dotted lines are the bound states of the potential and the corresponding wave functions are shown using solid lines. (b) The typical dependence of the phonon-induced dipole fluctuation spectrum of the adatom as a function of ω/Γ_0 , where Γ_0 is the characteristic transition rate from the first excited state to the ground state. The dipole fluctuation spectrum is in arbitrary units. The temperature is given in units of ν_{10} , the separation between the ground state and the first excited vibrational state. The inset shows the temperature dependence of the noise in the low- and high-frequency regions of the spectrum. See text and spectrum for more details.

of phonons creates a fluctuating dipole moment $\mu(t)$ as the adatom jumps between different levels $|n\rangle$. The dipole fluctuation in the transversal planar direction is ignored, because it leads to a different scaling of the heating noise with the distance of the ion from the trap electrodes and because most of the PDOS is concentrated in the normal to the surface.

B. Dipole fluctuation spectrum

From the above considerations and a detailed knowledge of the adatom-surface potential $U(z)$, the induced dipole moment $\mu(z)$, and the PDOS $g(\omega)$, we can evaluate the dipole fluctuation spectrum and thereby the corresponding ion heating rate Γ_h . The fluctuation spectrum is given by

$$S_\mu(\omega) = \int_{-\infty}^{\infty} d\tau [\langle \mu_z(\tau)\mu_z(0) \rangle - \langle \mu_z(0) \rangle^2] e^{i\omega\tau}, \quad (5)$$

where $\mu_z = \sum_n \mu_{z,n} p_n$ and $p_n = |n\rangle\langle n|$ is the projection operator on the vibrational level $|n\rangle$.

The typical dependence of $S_\mu(\omega)$ on frequency and temperature is shown in Fig. 1(b), establishing the rate $\Gamma_0 \equiv \Gamma_{1 \rightarrow 0}(T = 0)$ and the frequency $\nu_{10} \equiv (E_1 - E_0)/\hbar$ as the relevant scales in the problem. In Ref. [16] we used an

approximate analytic model to estimate the relevant scales for a broad range of adatom species, but assuming a clean gold surface. By using a harmonic approximation for $U(z)$ and assuming that $g(\omega) \sim \omega^2$ we obtain [16]

$$v_{10} \approx \zeta \sqrt{\frac{U_0}{mz_0^2}}, \quad \Gamma_0 \approx \frac{1}{4\pi} \frac{v_{10}^4 m}{v^3 \rho}, \quad (6)$$

where $\zeta \sim O(1)$ is a numerical constant, m is the mass of the adsorbate, ρ is the density of the slab, U_0 is the potential depth, and v is the speed of sound. The quadratic behavior of the PDOS is valid for low frequencies, and at higher frequencies the full form of PDOS must be used.

In the following we consider a more realistic scenario and evaluate the potential modifications of the dipole fluctuation spectrum due to the presence of an additional ML of atoms on top of the Au surface. To do so we present in the following section exact numerical calculations of adatom-surface potentials for the case of He and N MLs, which provides us with an estimate for the minimal and maximal expected modification of the surface potential. Approximate analytic expressions for Γ_0 given in Eq. (6) allow us to extend these predictions for various ML-adatom combinations.

III. ATOM-MONOLAYER-GOLD SURFACE INTERACTION

The asymptotic potential for a polarizable atom with dynamic polarizability $\alpha(\omega)$, which approaches a surface of dielectric constant ϵ , is $U(z \gg z_0) \simeq -\frac{(\epsilon-1)}{(\epsilon+1)} \frac{C_3}{z^3}$, where $C_3 = \frac{1}{4\pi} \int \alpha(i\omega) d\omega$ and z is the normal to the surface. As the atom approaches the surface, the interaction energy increases and the energy cost of the electronic exchange between the electrons of the adsorbate atom and the bulk atom becomes too great to overcome, leading to a repulsive wall in the interaction potential. Below, we present *ab initio* calculations of the interaction potential energies normal to the substrate surface of H atoms with a ML of adsorbate atoms He and N on top of the Au(111) surface.

A. ML surface interaction potentials

Total-energy calculations of bulk Au and Au(111) surfaces, with and without He and N adsorbate atoms, were performed using the spin-polarized DFT as implemented in the Vienna *Ab initio* Software Package (VASP) [18]. The exchange correlation energy was calculated using the local gradient approximation (LDA) with the parametrization of Perdew and Wang (PWC) [19].

The interaction between valence electrons and ionic cores has been described by the projector augmented wave (PAW) method [20,21]. The Au $5d^{10}6s^1$, N $2s^22p^3$, and He $1s^2$ electrons were treated explicitly as valence electrons in Kohn-Sham (KS) equations and the remaining cores were represented by PAW pseudopotentials. The KS equations were solved using the blocked Davidson iterative matrix diagonalization scheme followed by the residual vector minimization method. The plane-wave cutoff energy for the electronic wave functions was set to 500 eV.

All structures were optimized with periodic boundary conditions applied using the conjugate gradient method,

accelerated using the Methfessel-Paxton [22] Fermi-level smearing with a width of 0.2 eV. The total energy of the system and the Hellmann-Feynman forces acting on atoms were calculated with convergence tolerances set to 10^{-3} eV and 0.01 eV/Å, respectively. Structural optimizations and property calculations were carried out using the Monkhorst-Pack special k -point scheme [23] with $11 \times 11 \times 11$ and $7 \times 7 \times 1$ meshes for integrations in the Brillouin zone (BZ) of bulk and slab systems, respectively.

The supercell consisted of a three-layer thick gold slab with (111) orientation and a $p(2 \times 2)$ mesh unit, covered by He or N adsorbate atoms on one side of the slab model. The calculated lattice constant of bulk Au was 4.06 Å, in close agreement with the experimental value of 4.0780 Å at 25 °C [24]. The lattice parameters of the $p(2 \times 2)$ Au(111) surface constructed by cleaving the optimized bulk structure were $a = b = 5.74$ Å and $c = 25.00$ Å, with ca. 20.00 Å vacuum separating slabs, and $\alpha = \beta = 90^\circ$ and $\gamma = 120^\circ$. Although a large vacuum region (ca. 20 Å) was used between periodic slabs, the creation of dipoles upon adsorption of atoms on only one side of the slab can lead to spurious interactions between the dipoles of successive slabs. In order to circumvent this problem, a dipole correction was applied by means of a dipole layer placed in the vacuum region following the method outlined by Neugebauer and Scheffler [25].

The He-Au(111) and N-Au(111) interaction potentials were calculated by gradually moving a single He or N atom along the z axis normal to the Au(111) surface.

B. Atomic adsorption on Au(111)

Four different atomic adsorption sites are possible on a Au(111) surface: (1) a bridge site between two gold atoms, (2) on top of a gold atom, (3) in a hollow site between three gold atoms, termed a hexagonal-close-packed (hcp) site when there is a gold atom in the layer directly beneath the surface layer, or (4) a face-centered-cubic (fcc) site when there is a hole in the layer directly beneath the surface layer.

Total-energy calculations indicate that a single He atom adsorbs preferentially at the bridge site ($E = -48.760$ eV), slightly more energetically favorable than at the top site (-48.756 eV), the fcc site (-48.755 eV), and the hcp site (-48.749 eV). The elongated equilibrium He-Au bond distance of 3.58 Å suggests that He at the bridge site is weakly physisorbed to the Au(111) surface. For the adsorption of a single N atom, the fcc site is energetically preferred ($E = -70.393$ eV) over the hcp site ($E = -69.792$ eV), the bridge site (-69.098 eV), and the top site ($E = -66.510$ eV). Contrasting with the He adsorbate, the N atom occupying the fcc site appears chemisorbed to the Au(111) surface with a short N-Au bond distance of 2.05 Å.

Figure 2 shows the adsorbate potentials of H on the bare Au surface and in the presence of an additional ML of He and N. Note that we have shifted the potentials so that $E(z_0 \rightarrow \infty) = 0$. The presence of the weakly adsorbed He results in a much shallower potential while the chemisorbed N has the opposite effect, creating a deeper well that supports more bound states.

C. Atomic diffusion on Au(111)

Although our primary focus in this work is on dipole fluctuations induced by atomic motion perpendicular to the

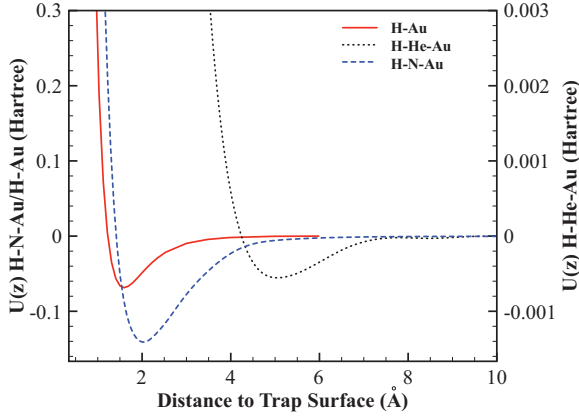


FIG. 2. (Color online) The binding potentials for H adsorbate atoms on bare Au surface (solid) and Au surface covered with one ML of He (dotted) or one ML of N (dashed). The peak of the local potential at the position of the first Au layer, in direct contact with the N(He) ML, does (not) vary appreciably, indicating the formation of a sizable (negligible) dipole moment. One hartree = 27.21 eV.

surface, the numerical data obtained in the previous part allows us with no additional effort to evaluate the diffusion rates of adatoms parallel to the surface. Such data could be relevant to other, diffusion-related noise processes [26–28] under identical conditions.

The surface diffusion coefficient is given by $D = \frac{\sqrt{3}}{4} r_0^2 \Gamma$ for an fcc(111) surface, where r_0 is the lattice parameter [2.87 Å for Au(111)] and Γ is the jump rate. Two different diffusion regimes exist, namely, a thermally activated regime and a quantum tunneling regime.

In the thermally activated regime, the thermal jump rate, Γ_{therm} , can be calculated through the Arrhenius formula [29],

$$\Gamma_{\text{therm}} = \gamma \exp\left(-\frac{E_a}{k_B T}\right), \quad (7)$$

where E_a is the activation energy barrier, k_B is the Boltzmann constant, T is the temperature, and γ is a prefactor which contains dynamical quantities; $\gamma \approx 10^{12} - 10^{13}$ Hz for most surfaces [30]. The diffusion of a He atom on Au(111) is expected to be nearly barrierless due to their weak physisorption interaction.

For the diffusion of a single N atom between adjacent stable fcc sites on Au(111) the activation energy was calculated in this study to be $E_a = 0.17$ eV using the nudged elastic band method within the DFT framework. This result is comparable to the value of ≈ 0.10 eV determined previously from experiment and theory for the diffusion of Cr on a Au(111) surface [31]. Following a simple Redhead's analysis of the migration temperature on solid surfaces [32], we estimate the temperature necessary for a N adatom to overcome this energy barrier to be ≈ 65 K [$E = 0.06T$ kcal mol $^{-1}$ K $^{-1}$]. Let us note that Redhead's law predicts the migration temperature of Cr adatoms on Au(111) to be 39 K, in excellent agreement with experimental findings [31]. The thermally activated diffusion jump rate of N on Au(111) at 65 K is calculated to be $\Gamma_{\text{therm}} = 0.3$ Hz for an activation energy of 0.17 eV and a prefactor $\gamma = 5 \times 10^{12}$ Hz; this corresponds to a surface

diffusion coefficient $D = 1.2 \times 10^{-16}$ cm 2 s $^{-1}$. At $T = 300$ K, $\Gamma_{\text{therm}} = 7 \times 10^9$ Hz and $D = 2.5 \times 10^{-6}$ cm 2 s $^{-1}$.

Below $T \approx 65$ K, thermally activated hopping is strongly suppressed, but adatoms can still diffuse via quantum tunneling. Although a full quantum treatment of surface diffusion is quite involved [33] a characteristic rate can be estimated from the tunneling rate between neighboring sites. For a one-dimensional parabolic double-well potential this rate can be approximated by [34]

$$\Gamma_{\text{tunnel}} = \frac{2\omega}{\pi^{3/2}} \sqrt{\frac{2E_a}{\hbar\omega}} \exp\left(-\frac{2E_a}{\hbar\omega}\right), \quad (8)$$

where $\omega = \sqrt{2E_a/mb^2}$ and b is the barrier width [$b = 0.8$ Å for Au(111)]. Therefore, the activation energy $E_a = 0.17$ eV corresponds to $\Gamma_{\text{tunnel}} \approx 70$ Hz, which dominates over thermally activated processes below temperatures of about 75 K. If the calculated E_a is considered to be accurate within ± 10 meV, Γ_{tunnel} can vary in the range $\approx 30 - 150$ Hz.

D. Work functions and surface dipoles

The work function, W , is defined as the minimum energy required to remove an electron from a solid to the vacuum region in the vicinity of the solid surface and is given by

$$W = \bar{V}(\infty) - E_F, \quad (9)$$

where $\bar{V}(\infty)$ is the plane-averaged electrostatic potential in the vacuum at a distance where the microscopic potential has reached its asymptotic value and E_F is the Fermi energy.

The electrostatic potential $V(x, y, z)$ on a grid in real space can be obtained from a self-consistent electronic structure calculation using a plane-wave basis set. The plane averaged potential is

$$\bar{V}(z) = \frac{1}{\mathcal{A}} \iint_{\text{cell}} V(x, y, z) dx dy, \quad (10)$$

where \mathcal{A} is the supercell surface area. The asymptotic value $\bar{V}(\infty)$ can be extracted by plotting the variation of \bar{V} as a function of z , as shown in Fig. 3 for a clean Au(111) surface and for a Au(111) surface covered by one ML of He and N atoms.

The calculated Fermi energy and electrostatic potential in the vacuum for the clean Au(111) surface are $E_F = -2.36$ eV and $\bar{V}(\infty) = +3.21$ eV. This corresponds to a work function $W_{\text{clean}} = 5.57$ eV, in good agreement with the experimental value of 5.50 eV recently measured by Bröker *et al.* [35] for this Miller index plane.

Adsorption of one ML of He atoms at bridge sites and N atoms at fcc sites onto the Au(111) surface results in $\bar{V}(\infty) = +3.24$ eV and $\bar{V}(\infty) = +4.68$ eV, respectively. Thus, the work functions of He- and N-covered Au(111) surfaces are $W_{\text{ads}} = 5.60$ and 7.04 eV.

In order to analyze the change of the work function upon atomic adsorption, we define the variation $\Delta W = W_{\text{ads}} - W_{\text{clean}}$. For the weakly physisorbed He ML this variation is negligible ($\Delta W = 0.03$ eV), unlike in the case of the chemisorbed N ML ($\Delta W = 1.47$ eV). The variation of the work function results from the change in the surface electric dipole caused by adsorption of the adatoms. Simple

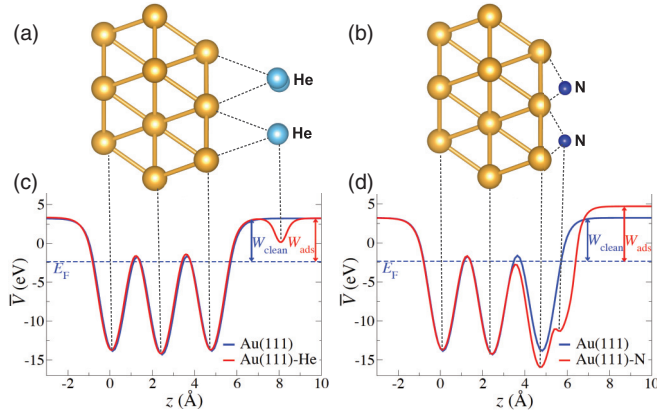


FIG. 3. (Color online) Au(111) slab models covered by a one-sided ML (one ML) of (a) He atoms and (b) N atoms. The variation of the corresponding plane averaged electrostatic potential $\bar{V}(z)$ along the z axis normal to the surface is represented for (c) He-covered and (d) N-covered Au(111) slabs, together with a clean Au(111) slab reference. The Fermi energy E_F (horizontal dashed line) and the work functions (vertical arrows) of the clean and adsorbate-covered slabs, W_{clean} and W_{ads} , respectively, are also represented.

electrostatics gives the relation [36]

$$\Delta W = \frac{e\Delta\mu}{\epsilon_0 A}, \quad (11)$$

where A is the surface area taken up by one adatom, ϵ_0 is the electric permittivity of free space, and $\Delta\mu$ is the change in surface dipole and is normalized per adatom. Since four adatoms form one ML covering the supercell surface area, the surface area by adatoms can be approximated by $A \approx \mathcal{A}/4$. We can now estimate the induced dipole moment for the case of He and N adsorbates. Using a DFT unit cell area of $\mathcal{A} \approx 41 \text{ \AA}^2$ we find $\mu_{\text{He}} \approx 0.03 \text{ D}$ while $\mu_{\text{N}} \approx 1.60 \text{ D}$.

It should be noted that the major contribution to the surface dipole results from the charge reordering associated with the formation of the chemical bonds between the metal surface and the adatoms. This contribution is foremost determined by the nature of the chemical bonds, but can also be modified by the packing density of the adatoms.

E. PDOS in the presence of the ML adsorbates

PDOS were calculated by solving the dynamical matrix for bulk Au, clean Au(111) surface, and adsorbates (e.g., He or N) on the Au(111) surface as shown in Fig. 4. A $(2 \times 2 \times 2)$ supercell was adopted to obtain the force constant matrix of bulk Au that can be derived from the Hellmann-Feynman forces obtained from the DFT calculations using VASP [18]. The calculated PDOS of the bulk Au shows two main peaks represented by ‘‘T’’ and ‘‘L’’ that are in good agreement with previous experimental results [37]. The longitudinal (L) and transverse (T) phonon modes of bulk Au are 4.61 and 2.75 THz, respectively, at a high symmetry point (X) in the Brillouin zone [37].

The calculated surface PDOS using the (2×2) supercells are depicted in Fig. 4(b) for a clean Au(111) surface as well as for one ML of adsorbates (He or N) on the Au(111) surface.

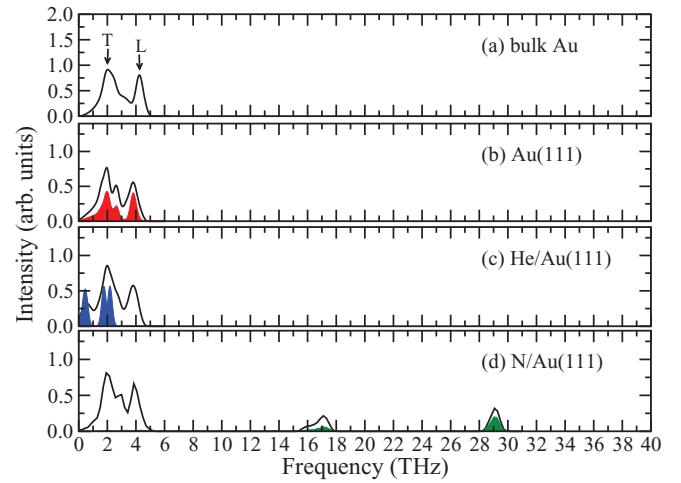


FIG. 4. (Color online) PDOS: (a) bulk Au, (b) bare Au(111) surface, (c) one ML He-covered Au(111) surface, and (d) one ML N-covered Au(111) surface. The curves in black are the calculated total PDOS and the shaded areas in red, blue, and green represent the partial PDOS projected to the surface atoms, He atoms, and N atoms, respectively. The peaks labeled by ‘‘T’’ and ‘‘L’’ refer to the transverse and longitudinal PDOS, respectively.

There are three prominent peaks in the calculated PDOS of the clean Au(111) surface, mainly contributed by the partial PDOS projected onto the surface atoms (red shaded area). The previous experimental study had identified four surface modes (2.31, 3.5, 4.0, and 4.3 THz) at a high symmetry point (K) in the surface Brillouin zone [38].

The calculated PDOS of the one ML He-covered Au(111) surface suggests a weak interaction between He and the metal surface, providing no evidence of stretching or wagging modes of He atoms with respect to the metal surface. However, the partial PDOS projected onto the He atoms (blue-shaded area) reveals the possible lattice modes of the one ML He atoms physisorbed on the surface as shown in Fig. 4(c).

Contrasting with the one ML He-covered Au(111) surface, two additional peaks appear at high frequency above 5 THz for the one ML N-covered Au(111) surface due to the wagging and stretching modes of N atoms attributed to the strong interaction with the metal surface, as shown in Fig. 4(d). The green-shaded area represents the partial PDOS projected onto the N atoms.

IV. NOISE SPECTRUM WITH ML PRESENT

Let us now evaluate the potential impact of different types of MLs on the dipole fluctuation spectrum of adatoms discussed in Sec. II. We first note that due to the high reactivity and low mass of H adsorbates—chosen in the previous section to reduce the DFT computational cost—the depth of the binding potential $U_{0,\text{bare}} = 1.85 \text{ eV}$ and the vibrational frequencies $\nu_{10,\text{bare}}/2\pi \approx 40 \text{ THz}$ are exceptionally high. Therefore, for H adatoms thermally activated processes at room temperature do not play a significant role. However, the same qualitative changes that occur in the surface potential for H are also expected for heavier adatoms or molecules and for the following estimates we simply use the potentials shown in Fig. 2 together with the mass scaling relations in Eq. (6)

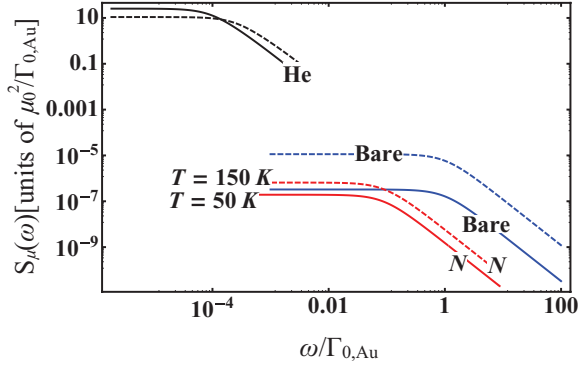


FIG. 5. (Color online) The dipole fluctuation spectrum $S_\mu(\omega)$ as a function of $\omega/\Gamma_{0,\text{Au}}$ for adsorbate of mass $m \sim 100$ amu on a He ML (black), a N ML (red), and a bare system (blue). For each system the solid curve corresponds to $T = 50$ K while the dashed curve corresponds to $T = 150$ K. The frequency ω is scaled by $\Gamma_{0,\text{Au}}$, the characteristic rate corresponding to the bare surface. The spectrum is given in units of $\mu_0^2/\Gamma_{0,\text{Au}}$, where μ_0 is the dipole moment of the adatom in the vibrational ground state.

to evaluate the noise spectrum for a more relevant range of adsorbate masses $m \sim 100$ amu.

In Fig. 5 we plot the dipole fluctuation spectrum $S_\mu(\omega)$ for a bare Au surface and in the presence of a He ML and a N ML. For these results we have assumed $m = 100$ amu and two different temperatures: $T = 50$ K (solid lines) and $T = 150$ K (dashed lines). The spectrum is given in units of $\mu_0^2/\Gamma_{0,\text{Au}}$, where μ_0 is the dipole moment of the adatom in the vibrational ground state and is typically around 1 D. $\Gamma_{0,\text{Au}}$ is the characteristic phonon-induced relaxation rate for the bare Au surface, which we use in all plots as a common frequency scale. For the bare Au surface where $z_0 \approx 1.59$ Å these values correspond to $\nu_{10}/2\pi \approx 4.5$ THz and ratios $k_B T/\hbar\nu_{10} \approx 0.20$ and 0.70 , respectively. The analytic estimate given in Eq. (6) predicts $\Gamma_{0,\text{Au}}/2\pi \approx 2.2$ THz, but from Fig. 4(b) we see that for these large vibrational frequencies the simple quadratic scaling of the PDOS already overestimates $\Gamma_{0,\text{Au}}$ by about a factor of 5–10 and more realistic values for $\Gamma_{0,\text{Au}}$ lie in the hundred GHz regime (for concreteness a value of $\Gamma_{0,\text{Au}}/2\pi = 250$ GHz is used for the plots in Fig. 5). For the assumed temperatures the dominant contribution of the noise comes from thermal excitations of the first excited vibrational state and the spectrum can be approximated by the Lorentzian

$$S_\mu(\omega) = (\mu_1 - \mu_0)^2 \frac{2\Gamma_0}{\Gamma_0^2 + \omega^2} e^{-\hbar\nu_{10}/k_B T}. \quad (12)$$

In Sec. III, we have found that due to its low reactivity, the He ML results in a significantly shallower well depth, $U_{0,\text{He}} = 14.9$ meV, shifting the minimum to $z_{0,\text{He}} \approx 5$ Å. Both effects lower the vibrational frequency, $\nu_{10,\text{He}} \approx 0.4$ THz, and lead to a drastic reduction of the characteristic phonon transition rate $\Gamma_{0,\text{He}}/2\pi \approx 150$ MHz. From Eq. (12) we see that this results in an increase of the low-frequency noise level, but reduces the noise at frequencies $\omega \gg \Gamma_0$. Interestingly, Fig. 4(c) shows that the projected PDOS of the He ML exhibits a sharp gap at frequencies around 0.5 THz. Since the adatom will be mainly affected by vibrations of the surface atoms, a strong variation of $\Gamma_{0,\text{He}}$ within this frequency range is expected.

The more reactive N ML results in a deeper potential well with $U_{0,\text{N}} = 3.8$ eV, while only slightly affecting the equilibrium distance, $z_{0,\text{N}} \approx 2$ Å. This leads to an increase of the vibrational frequency, $\nu_{10,\text{N}} \approx 5.3$ THz, and in general one would expect a corresponding increase of $\Gamma_{0,\text{N}}$. However, as shown in Fig. 4(c) the strong binding of N leads to drastic modifications in the projected PDOS since vibrations of the ML atoms are mismatched in frequency and strongly decoupled from the phonons in the bulk. At frequencies around a few THz the numerically evaluated projected PDOS for the N ML is about a factor of 100 smaller than for the bare Au surface and $\Gamma_{0,\text{N}} \approx \Gamma_{0,\text{Au}}/100 \approx 2\pi \times 2.5$ GHz. This is in contrast to a ML of similar reactivity, but matched phonon spectrum, where decay rates of $\Gamma_0 \sim 0.5$ –1 THz are expected.

V. SUMMARY AND CONCLUSIONS

In summary, we have calculated the noise-induced heating in ion traps due to randomly fluctuating adatom dipoles in the presence of a single ML of atomic species on a Au(111) surface. Precise DFT calculations of surface potentials for physisorbed and chemisorbed ML species provided us with accurate data for surface potentials and PDOS from which the effects on the noise could be evaluated. We have found that within our noise model, the presence of surface contamination can lead to drastic modifications and, depending on the reactivity of the ML species, the PDOS and the frequency range either enhance or reduce the noise level.

Although an exact quantitative comparison between experiments, for example, in Refs. [12,13], is beyond the scope of this work, our current analysis clearly illustrates the impact of various different surface properties on the overall level of the noise and suggests new ways to suppress anomalous heating in ion traps by a controlled ML deposition. In particular, we found that a weakly reactive ML with a phonon spectrum that is mismatched with that of gold can lead to a strong increase in the low-frequency noise, while the opposite is true for a highly reactive layer with a matched phonon spectrum. Further, the combined data on surface potentials, PDOS, and diffusion rates obtained in this work could in the future serve as a common input to evaluate and compare different alternative noise models. This could lead to better understanding of the noise mechanism, allowing ion traps to be used as exquisite probes of surface reactivity.

ACKNOWLEDGMENTS

Sandia National Laboratories is a multiprogram laboratory managed and operated by Sandia Corporation, a wholly owned subsidiary of Lockheed Martin Corporation, for the US Department of Energy's National Nuclear Security Administration under Contract No. DE-AC04-94AL85000. P.R. acknowledges support by the Austrian Academy of Sciences and the Austrian Science Fund (FWF) through START Grant No. Y 591-N16. This work was supported by NSF through a grant to ITAMP at the Harvard-Smithsonian Center for Astrophysics.

- [1] H. Haeffner, C. F. Roos, and R. Blatt, *Phys. Rep.* **469**, 155 (2008).
- [2] D. J. Wineland and D. Leibfried, *Laser Phys. Lett.* **8**, 175 (2011).
- [3] D. J. Wineland, C. Monroe, W. M. Itano, D. Leibfried, B. E. King, and D. M. Meekhof, *J. Res. Natl. Inst. Stand. Technol.* **103**, 259 (1998).
- [4] R. G. DeVoe and C. Kurtsiefer, *Phys. Rev. A* **65**, 063407 (2002).
- [5] Q. A. Turchette, D. Kielpinski, B. E. King, D. Leibfried, D. M. Meekhof, C. J. Myatt, M. A. Rowe, C. A. Sackett, C. S. Wood, W. M. Itano, C. Monroe, and D. J. Wineland, *Phys. Rev. A* **61**, 063418 (2000).
- [6] L. Deslauriers, P. C. Haljan, P. J. Lee, K.-A. Brickman, B. B. Blinov, M. J. Madsen, and C. Monroe, *Phys. Rev. A* **70**, 043408 (2004).
- [7] L. Deslauriers, S. Olmschenk, D. Stick, W. K. Hensinger, J. Sterk, and C. Monroe, *Phys. Rev. Lett.* **97**, 103007 (2006).
- [8] R. J. Epstein *et al.*, *Phys. Rev. A* **76**, 033411 (2007).
- [9] J. Labaziewicz, Y. Ge, P. Antohi, D. Leibbrandt, K. R. Brown, and I. L. Chuang, *Phys. Rev. Lett.* **100**, 013001 (2008); J. Labaziewicz, Y. Ge, D. R. Leibbrandt, S. X. Wang, R. Shewmon, and I. L. Chuang, *ibid.* **101**, 180602 (2008).
- [10] S. X. Wang, Y. Ge, J. Labaziewicz, E. Dauler, K. Berggren, and I. L. Chuang, *Appl. Phys. Lett.* **97**, 244102 (2010).
- [11] N. Daniilidis, S. Narayanan, S. A. Möller, R. Clark, T. E. Lee, P. J. Leek, A. Wallraff, St. Schulz, F. Schmidt-Kaler, and H. Häffner, *New J. Phys.* **13**, 013032 (2011).
- [12] D. T. C. Allcock, L. Guidoni, T. P. Harty, C. J. Ballance, M. G. Blain, A. M. Steane, and D. M. Lucas, *New J. Phys.* **13**, 123023 (2011).
- [13] D. A. Hite *et al.*, *Phys. Rev. Lett.* **109**, 103001 (2012).
- [14] R. Dubessy, T. Coudreau, and L. Guidoni, *Phys. Rev. A* **80**, 031402 (2009).
- [15] G. H. Low, P. F. Herskind, and I. L. Chuang, *Phys. Rev. A* **84**, 053425 (2011).
- [16] A. Safavi-Naini, P. Rabl, P. F. Weck, and H. R. Sadeghpour, *Phys. Rev. A* **84**, 023412 (2011).
- [17] P. R. Antoniewicz, *Phys. Rev. Lett.* **32**, 1424 (1974).
- [18] G. Kresse and J. Furthmüller, *Phys. Rev. B* **54**, 11169 (1996).
- [19] J. P. Perdew and Y. Wang, *Phys. Rev. B* **45**, 13244 (1992).
- [20] P. E. Blöchl, *Phys. Rev. B* **50**, 17953 (1994).
- [21] G. Kresse and D. Joubert, *Phys. Rev. B* **59**, 1758 (1999).
- [22] M. Methfessel and A. T. Paxton, *Phys. Rev. B* **40**, 3616 (1989).
- [23] H. J. Monkhorst and J. D. Pack, *Phys. Rev. B* **13**, 5188 (1976).
- [24] B. N. Dutta and B. Dayal, *Phys. Stat. Sol. (b)* **3**, 473 (1963).
- [25] J. Neugebauer and M. Scheffler, *Phys. Rev. B* **46**, 16067 (1992).
- [26] M. A. Gesley and L. W. Swanson, *Phys. Rev. B* **32**, 7703 (1985).
- [27] G. W. Timm and A. Van der Ziel, *Physica* **32**, 1333 (1966).
- [28] C. Henkel and B. Horowitz, *Phys. Rev. A* **78**, 042902 (2008).
- [29] S. Arrhenius, *Z. Phys. Chem. (Leipzig)* **4**, 226 (1889).
- [30] S. Ovesson, A. Bogicevic, G. Wahnström, and B. I. Lundqvist, *Phys. Rev. B* **64**, 125423 (2001).
- [31] P. Ohresser, H. Bulou, S. S. Dhesi, C. Boeglin, B. Lazarovits, E. Gaudry, I. Chado, J. Faerber, and F. Scheurer, *Phys. Rev. Lett.* **95**, 195901 (2005).
- [32] R. I. Masel, *Principles of Adsorption and Reaction on Solid Surfaces* (Wiley, New York, 1996).
- [33] V. Pouthier and J. C. Light, *J. Chem. Phys.* **113**, 1204 (2000).
- [34] E. Merzbacher, *Quantum Mechanics* (Wiley, New York, 1970).
- [35] B. Bröker, R.-P. Blum, J. Frisch, A. Vollmer, O. T. Hofmann, R. Rieger, K. Müllen, J. P. Rabe, E. Zojer, and N. Koch, *Appl. Phys. Lett.* **93**, 243303 (2008).
- [36] J. D. Jackson, *Classical Electrodynamics* (Wiley, New York, 1975).
- [37] J. W. Lynn, H. G. Smith, and R. M. Nicklow, *Phys. Rev. B* **8**, 3493 (1973).
- [38] M. W. G. Ponjee, C. F. J. Flipse, A. W. Denier van der Gon, and H. H. Brongersma, *Phys. Rev. B* **67**, 174301 (2003).